Reactions of *Mycobacterium tuberculosis* Truncated Hemoglobin O with Ligands Reveal a Novel Ligand-Inclusive Hydrogen Bond Network†

Hugues Ouellet,‡ Laura Juszczak,§ David Dantsker,§ Uri Samuni,§ Yannick H. Ouellet,‡ Pierre-Yves Savard,‡ Jonathan B. Wittenberg,§ Beatrice A. Wittenberg,§ Joel M. Friedman,§ and Michel Guertin*,‡

Department of Biochemistry and Microbiology, Faculty of Sciences and Engineering, Laval University, Quebec, Quebec G1K 7P4, Canada, and Department of Physiology and Biophysics, Albert Einstein College of Medicine, Bronx, New York 10461

Received October 18, 2002; Revised Manuscript Received February 17, 2003

ABSTRACT: Truncated hemoglobin O (trHbO) is one of two trHbs in *Mycobacterium tuberculosis*. Remarkably, trHbO possesses two novel distal residues, in addition to the B10 tyrosine, that may be important in ligand binding. These are the CD1 tyrosine and G8 tryptophan. Here we investigate the reactions of trHbO and mutants using stopped-flow spectrometry, flash photolysis, and UV-enhanced resonance Raman spectroscopy. A biphasic kinetic behavior is observed for combination and dissociation of O_2 and CO that is controlled by the B10 and CD1 residues. The rate constants for combination (<1.0 μM^{-1} s^{-1}) and dissociation (<0.006 s^{-1}) of O_2 are among the slowest known, precluding transport or diffusion of O_2 as a major function. Mutation of CD1 tyrosine to phenylalanine shows that this group controls ligand binding, as evidenced by 25- and 77-fold increases in the combination rate constants for O_2 and CO, respectively. In support of a functional role for G8 tryptophan, UV resonance Raman indicates that the $\chi^{(2,1)}$ dihedral angle for the indole ring increases progressively from approximately 93° to at least 100° in going sequentially from the deoxy to CO to O_2 derivative, demonstrating a significant conformational change in the G8 tryptophan with ligation. Remarkably, protein modeling predicts a network of hydrogen bonds between B10 tyrosine, CD1 tyrosine, and G8 tryptophan, with the latter residues being within hydrogen bonding distance of the heme-bound ligand. Such a rigid hydrogen bonding network may thus represent a considerable barrier to ligand entrance and escape. In accord with this model, we found that changing CD1 or B10 tyrosine for phenylalanine causes only small changes in the rate of O_2 dissociation, suggesting that more than one hydrogen bond must be broken at a time to promote ligand escape. Furthermore, trHbO−CO cannot be photodissociated under conditions where the CO derivative of myoglobin is extensively photodissociated, indicating that CO is constrained near the heme by the hydrogen bonding network.

Truncated hemoglobins (trHbs)[1] constitute a class of small O_2-binding heme proteins distributed in eubacteria, cyanobacteria, protozoa, and plants; they are a separate group within the hemoglobin (Hb) superfamily. Three phylogenetic groups (groups I−III) are distinguished within the trHb family (*1*).

Although trHbs bind O_2 reversibly, they differ both in their ligand binding and in their structures from animal myoglobins (Mb) and Hbs. Novelty resides in a pattern of unusual ligand reactivity, an unprecedented two-over-two α-helical sandwich variation of the classical three-over-three α-helical sandwich motif common to almost all other Mbs and Hbs, a complex ligand-inclusive H-bonding network within the distal heme pocket, and a consistent presence of an extended hydrophobic tunnel/cavities network linking the solvent to the distal heme pocket (*2*−*9*).

In *Mycobacterium tuberculosis* and *Mycobacterium bovis*, two genes, *glbN* and *glbO*, encode distantly related trHbs from group I (trHbN) and group II (trHbO), respectively (*1*). The extent of amino acid identity between the two proteins is only 18%. Studies performed with *M. bovis bacillus* Calmette-Guérin (BCG) demonstrated that trHbO is expressed throughout the growth phase, but in contrast, trHbN expression is greatly enhanced during the stationary phase (*6*, *10*), suggesting different functions. Disruption of *glbN* in *M. bovis* BCG caused a dramatic reduction in the NO-consuming activity of stationary phase cells and caused aerobic respiration to be markedly inhibited by NO compared to that of wild-type (WT) cells, indicating a protective function for trHbN (*11*). In a recent paper, Pathania et al. (*12*) showed that trHbN can also protect *Escherichia coli* against nitrosative stress. Although Pathania et al. (*13*) claimed trHbO enhances O_2 uptake of *E. coli* membrane fractions, no physiological function has been demonstrated.

† This work was supported by Natural Sciences and Engineering Research Council of Canada Grant 46306-01 (to M.G.) and by NIH Grants R01 EB00296 and P01 GM58890 (to J.M.F.).

* To whom correspondence should be addressed. Telephone: (418) 656-2131, ext. 5581. Fax: (418) 656-7176. E-mail: mguertin@bcm.ulaval.ca.

‡ Laval University.

§ Albert Einstein College of Medicine.

[1] Abbreviations: trHb, truncated hemoglobin; BCG, bacillus Calmette-Guérin; Hb, hemoglobin; Mb, myoglobin; UVRR, UV resonance Raman.

10.1021/bi0270337 CCC: $25.00
Published on Web 04/26/2003

trHbN displays high affinity for O_2 due to a fast combination (25 μM^{-1} s^{-1}) and slow dissociation (0.2 s^{-1}) (*6*). In trHbN, a distal network of H-bonds stabilizes the ligated O_2 through direct interaction with the phenolic oxygen atom of B10Tyr and H-bonding of this oxygen atom to E11Gln (*8*). When B10Tyr is mutated to Phe, the O_2 dissociation rate increases 125-fold (*6*). In trHbN, E7Leu cannot form a H-bond to the heme-bound ligand. Resonance Raman studies, in conjunction with site-directed mutagenesis, indicated that B10Tyr interacts strongly with the heme-bound O_2, and suggested that trHbN heme iron coordination may be optimized for performing O_2/NO chemistry (*14*). In line with these observations, we found that the second-order rate constant for the reaction between trHbN$-O_2$ and NO at 23 °C was 745 μM^{-1} s^{-1}, 20-fold greater than that for Mb, and that B10Tyr is necessary for the reaction of trHbN$-O_2$ with NO (*11*).

We return to trHbO. Structure-based sequence alignment (*1*) suggests that the E7 and B10 positions are Ala and Tyr, respectively. At position E11, a non-hydrogen bond donor, Leu, is found. The residue at position CD1, which is Phe in trHbs from group I and group III and in several group II trHbs, is Tyr (*1*). Phe is invariably found at position CD1 in animal Hbs and Mbs. Remarkably, CD1Tyr is shared by group II trHbs from high-guanosine/cytosine, Gram-positive bacteria (*M. tuberculosis*, *Mycobacterium avium*, *Mycobacterium leprae*, *Cornybacterium diphteriae*, *Cornybacterium glutamicum*, *Streptomyces coelicolor*, and *Thermobifida fusca*), supporting a functional role for CD1Tyr.

In common with all trHbs from group II and group III, trHbO has a Trp residue at position G8. Smaller apolar residues (Val, Leu, or Ile) are found in group I trHbs. In Mb, G8Ile is among the residues that define Xenon cavity 4 (*15*, *16*). Studies of sperm whale Mb mutants show that the size of the side chain residue at the G8 position plays a role in controlling ligand diffusion between the distal heme pocket and the adjacent Xenon cavity 4 (*16*−*18*). On the basis of the geminate and nongeminate kinetic patterns observed in Mb mutants and *Ascaris* Hb (G8Phe), it was concluded that large residues at the G8 position impede the escape of dissociated ligands from the distal heme pocket into Xenon cavity 4 (*18*−*20*). As a result, there is an increase in the geminate yield and a decrease in the rate of ligand dissociation from the heme. The presence of a large polar Trp at position G8 is likely to be important in controlling ligand binding in group II trHbs. Furthermore, the proximity of G8 to other key elements within the distal heme pocket, such as the heme-bound ligand and residues B10 and CD1, raises the prospect that G8Trp may be strongly coupled to the H-bonding network described below that contributes to the control of ligand reactivity.

In trHbO$-O_2$, strong polar interactions stabilize the heme-bound O_2, as evidenced by a relatively low frequency of the Fe$-O_2$ stretching mode (559 cm^{-1}) (*10*). However, mutagenesis of B10Tyr or CD1Tyr to Phe made only very small changes in the Fe$-O_2$ stretching mode. To explain these results, it was proposed that in mutants the distal heme pocket is rearranged so that either the B10 or CD1 residue can still stabilize the heme-bound ligand. At that time, G8Trp was not considered a residue that could stabilize heme-bound ligands. The presence of a H-bond between CD1Tyr and the proximal oxygen atom of the heme-bound O_2 was shown to account for the unusual observed O−O stretching frequency.

Here we investigate the reactions of ligands with trHbO and the roles of B10Tyr, CD1Tyr, and G8Trp in ligand binding. The results indicate that trHbO differs considerably from trHbN in ligand binding properties, and are compatible with a rigid network of H-bonds between CD1, B10, and G8 residues controlling ligand binding. The findings greatly limit the functional options for trHbO.

EXPERIMENTAL PROCEDURES

Purification of Recombinant trHbO. Recombinant trHbO and mutants were purified as previously described (*10*).

Anaerobic Conditions. Sample preparation and stopped-flow spectrophotometric experiments were carried out in a glovebox (LabMaster 100, MBraun Inc.), equipped with a catalytic purifier that maintained the oxygen content at ≤3 ppm. Aqueous solutions in equilibrium with this gas mixture would be 4 nM in oxygen.

Preparation of NO-Saturated Solutions. NO-saturated solutions were prepared as previously described (*11*). The NO concentration in buffer was routinely determined using an NO electrode (World Precision Instruments, Sarasota, FL) and equals 1500−2000 μM.

Preparation of trHbO Derivatives. Solutions of deoxy trHbO were prepared by first flushing solutions of ferric protein with N_2 for 20 min. The protein was then reduced inside the glovebox with a 10-fold molar excess of sodium dithionite and desalted by passage through a P6DG column equilibrated with anaerobic buffer. Working concentrations, monitored spectrophotometrically, were achieved by diluting the protein solution with anaerobic buffer in gastight syringes.

Solutions of trHbO$-O_2$, trHbO−CO, and trHbO−NO were prepared in gastight syringes sealed with a septum by injecting solutions of the deoxy derivative into the appropriate volumes of solutions saturated with either O_2 (1200 μM in buffer), CO (1000 μM in buffer), or NO (1500−2000 μM in buffer).

Optical Absorption Spectroscopy. Optical absorption spectra were recorded using a Cary model 3E spectrophotometer (Varian) equipped with a temperature-controlled multicell holder as previously described (*10*).

Determination of the Molecular Mass of trHbO. The state of aggregation of trHbO was investigated by gel filtration at 23 °C using the ÄKTA *FPLC* protein purification system (Amersham Pharmacia Biotech). One hundred microliters of deoxy, O_2, and met derivatives of trHbO (0.15 mg/mL) were applied to a Superdex 75 HR 10/30 column (Amersham Biosciences) equilibrated with 10 mM Tris-HCl buffer (pH 7.5) containing 50 μM EDTA and either 15, 75, 150, or 300 mM NaCl and eluted with the same buffers at a flow rate of 0.9 mL/min. Before injection, the protein samples were equilibrated against the same buffers by dialysis. For the deoxy derivative of trHbO, the elution buffer also contained 1 mM sodium dithionite, and chromatography was performed in the glovebox. A gel filtration standard (Bio-Rad), a lyophilized mixture of thyroglobulin (1 mg), bovin gamma globulin (1 mg), chicken ovalbumin (1 mg), heart horse myoglobin (0.5 mg), and vitamin B_{12} (0.1 mg), was used to calibrate the column. The standards were dissolved in 100 μL of the appropriate buffers. Elution profiles were moni-

tored at 280 and 405 nm. Exclusion and retention volumes were calculated using Unicorn version 3.4 (Amersham Biosciences). No change in the elution volume of the molecular mass standards was observed when the ionic strength of the buffer was varied.

The proportion of monomer was calculated using the following equation (*21*):

$$M_w = M_m([M] + 4[M2])/[M] + 2[M2]$$

M_w is the weight-average molecular mass, and M_m is the molecular mass of the monomer (14.9 kDa). [M] and [M2] are the equilibrium concentrations of the monomer and dimer, respectively.

Ligand Reaction Rates. Rapid mixing experiments were conducted with an Applied Photophysics (Leatherhead, U.K.) SX.18MV single-wavelength stopped-flow spectrophotometer equipped with a photodiode array detector. To reproducibly achieve satisfactory anaerobic conditions, the sample handling unit was placed inside the glovebox. Rates were computed using Olis Globalworks software (OLIS, Bogart, GA). All the reaction kinetics were measured at 23 °C, unless specified, in 50 mM potassium phosphate buffer (pH 7.5) containing 50 μM EDTA. Traces (averages of at least five single traces) from at least three experiments were averaged to obtain each observed rate constant.

O_2 Combination Rate. Solutions of deoxy trHbO (5.0 μM heme in buffer) were mixed rapidly with solutions of O_2 (50−1000 μM in buffer), and the reaction was followed at 436 and 410 nm, a minimum and a maximum in the trHbO−O_2 minus deoxy trHbO difference spectrum, respectively. Six O_2 concentrations were used.

CO Combination Rate. Solutions of deoxy trHbO (5.0 μM heme in buffer) were mixed rapidly with solutions of CO (50−1000 μM in buffer), and the reaction was followed at 418 and 437 nm, a maximum and a minimum in the trHbO−CO minus deoxy trHbO difference spectrum, respectively. Six CO concentrations were used.

NO Combination Rate. Solutions of deoxy trHbO (5.0 μM heme in buffer) were mixed rapidly with solutions of NO (50−500 μM in buffer), and the reaction was followed at 437 nm, a minimum in the trHbO−NO minus deoxy trHbO difference spectrum. Six NO concentrations were used.

O_2 Dissociation Rate. Solutions of trHbO−O_2 (5 μM HbO_2, 10 μM free O_2 in buffer) were mixed rapidly with a solution of CO (1000 μM in buffer), and the reaction was followed at 420 and 405 nm, a maximum and a minimum in the trHbO−CO minus trHbO−O_2 difference spectrum, respectively. The dissociation rates were calculated as the reaction approached equilibrium using the equation $k_{O_2} = k_{obs}(1 + k'_{O_2}/l'_{CO})[O_2]/[CO]$ (*22*). The rate was independent of CO concentration from 250 to 500 μM, after mixing.

In separate experiments, solutions of trHbO−O_2 (5 μM HbO, 10 μM free O_2 in buffer) were mixed rapidly with solutions of sodium dithionite or with solutions of *n*-butylisocyanide (~40 mM in buffer before mixing) containing sodium dithionite. The reaction with sodium dithionite alone was followed at 436 and 410 nm, a maximum and a minimum in the deoxy trHb minus trHbO−O_2 difference spectrum, respectively. Reactions in the presence of *n*-butylisocyanide were followed at 429 nm, a maximum in the ferrous *n*-butylisocyanide trHb adduct minus trHbO−O_2 difference spectrum. The reactions followed first-order kinetics to more than 90% completion.

CO Dissociation Rate. Solutions of trHbO−CO (5 μM HbCO, 10 μM free CO in buffer) were mixed rapidly with a solution of O_2 (1200 μM in buffer), and the reaction was followed at 405 and 420 nm, a maximum and a minimum in the trHbO−O_2 minus trHbO−CO difference spectrum, respectively. The rate was independent of O_2 concentration from 250 to 500 μM. The dissociation rates were calculated using the equation $l_{CO} = k_{obs}(1 + l'_{CO}/k'_{O_2})[CO]/[O_2]$ (*22*).

Partition of M. tuberculosis trHbO between O_2 and CO. A solution of trHbO−O_2 (7 μM heme in 50 mM potassium HEPES buffer (pH 7.5) containing 50 μM EDTA) was equilibrated at a total pressure of 1 atm with wet gas mixtures containing various proportions of O_2 and CO. The trHbO−CO and trHbO−O_2 species were the only forms present, at a significant concentration. Formation of ferric Mb was not detectable during the measurements. After equilibration for 20−40 min at each gas composition, optical spectra were acquired from 470 to 380 nm, using a modified (Aviv Associates, Lakewood, NJ) Cary model 17 recording spectrophotometer equipped with a temperature-controlled cell holder. Calculations were made from the sum of the changes at 421 and 407 nm, wavelengths of the maximum change in the trHbO−CO minus trHbO−O_2 difference spectrum.

Stopped-Flow Kinetic Analysis of the NO-Induced Oxidation of trHbO−O_2. Kinetic studies were carried out as previously described (*11*). The kinetic traces were recorded at 396 nm, a maximum in the trHbO-met minus trHbO−O_2 difference spectrum.

Geminate Recombination and Bimolecular Recombination. Geminate and solvent phase recombination measurements were carried out using 8 ns 532 nm pulses at 1 Hz from a Nd:YAG laser (Minilite, Continuum, Santa Clara, CA) as a photodissociation source and a greatly attenuated CW probe beam at 442 nm. Samples were placed in a custom-designed variable-temperature holder that allows for temperature tuning between −15 and 70 °C.

UV-Enhanced Resonance Raman Spectroscopy. UV resonance Raman (UVRR) data were collected on samples cooled to 10 ± 4 °C to minimize photodamage. The excitation wavelength was 229 nm, and the incident laser power was 1.8 mW. Four 3 min acquisitions accumulated for each ligation state over a frequency window of 820−1670 cm^{-1}. Absorption spectra were collected before and after exposure to the UV laser beam. If absorption changes were noted, the sequential UV resonance Raman acquisitions were examined for evidence of band changes. Acquisitions that showed changes were rejected and not included in the final UV resonance Raman average spectra. Spectral data were truncated to a frequency window focused on the W3 band (~1558 cm^{-1}) for each set of spectra. The most substantial ligation-specific changes in the spectrum are associated with this band. A detailed account of the spectrum will be presented in a future publication. The frequency of this tryptophan band is sensitive to the $\chi^{(2,1)}$ angle of the indole ring and as such is an excellent probe of conformational changes associated with tryptophans. The software program Grams/32 AI, version 6.00 (Galactic Industries Corp., Salem, NH), was used for curve fits to the W3 band, allowing for deconvolution of W3 into contributing bands.

Computational Models and Methods. The computational modeling of the deoxy form, O_2, and CO derivatives of trHbO was done following a three-step method using version 2000.1 of Insight II of Accelrys Inc. (*23*). The crystal structure of subunit B of trHbN−O_2 (PDB entry 1idr) was used as a template. Using the Biopolymer module, CD1Phe, E7Leu, and G8Val were substituted with Tyr, Ala, and Trp, respectively. The first step involved assignment of the ESFF force field potentials and partial charges. In the second step, a 5 Å water layer was added. The systems for trHbO−O_2 and trHbO−CO were composed of 4635 total atoms, 1990 protein atoms, 881 water molecules, and two ligand atoms. The third step involved the computational simulation using version 98 of the Discover3 module. The simulation started by fixing the protein and allowing the water layer molecules to relax using an energy minimization step of ∼1500 iterations with the steepest descent and conjugated gradient algorithms. Then a 6 ps dynamic at 300 K with a time step of 1 fs was performed to reorient the solvent molecules. Afterward, minimization using the conjugated gradient algorithm was done in six stages. During minimization, the atomic coordinates of the protein backbone atoms and heme atoms were restrained to their initial positions using a quadratic penalty function. The penalty function force constant was decreased from 1000 to 2 kcal mol^{-1} Å^{-1} until it was finally removed, and the system was minimized for 100−2000 iterations at each step. Finally, the protein was relaxed at 0 K using a minimization step performed with the conjugated gradient algorithm.

RESULTS

State of Aggregation of trHbO. Before investigating the kinetics of ligand binding to trHbO, we examined the state of aggregation of the oxy, deoxy, and ferric protein (15 μg each) by gel filtration at pH 7.5 and 23 °C in a buffer containing 10 mM Tris-HCl and various concentrations of NaCl. As shown in Figure 1A, ferric trHbO eluted as a single symmetrical peak in the range of 15−20 kDa at different salt concentrations. The apparent molecular mass of ferric trHbO was 20 kDa under low-salt conditions (15 mM NaCl) and decreased with increasing ionic strength to a value close to that expected for the monomeric protein (14.9 kDa) in 300 mM NaCl (Figure 1B). Nearly identical results were obtained for the oxy and deoxy protein. The symmetrical shape of the elution peak obtained under the latter conditions indicated that association−dissociation reactions at equilibrium are very fast at 23 °C. This has been reported for other proteins (*24*−*26*). These molecular masses were used to calculate the corresponding monomer/dimer ratios of trHbO. While trHbO existed in a monomer/dimer ratio of 79/21 in 15 mM NaCl, only monomer was present at 300 mM NaCl. In 50 mM phosphate, the buffer used in the kinetic analysis, the monomer/dimer ratio (96/4) indicates that monomer largely dominates.

Reactions with Ligands. It must be stressed here that optical absorption and resonance Raman spectra of trHbO, the B10Tyr → Phe mutant, and the CD1Tyr → Phe mutant indicate that these species are five-coordinate in the deoxy state (*10*). No significant differences were observed in the reaction of ligands with either monomeric or dimeric trHbO.

O_2 Combination. The time course of O_2 combination with wild-type deoxy trHbO is shown in Figure 2A. The curve

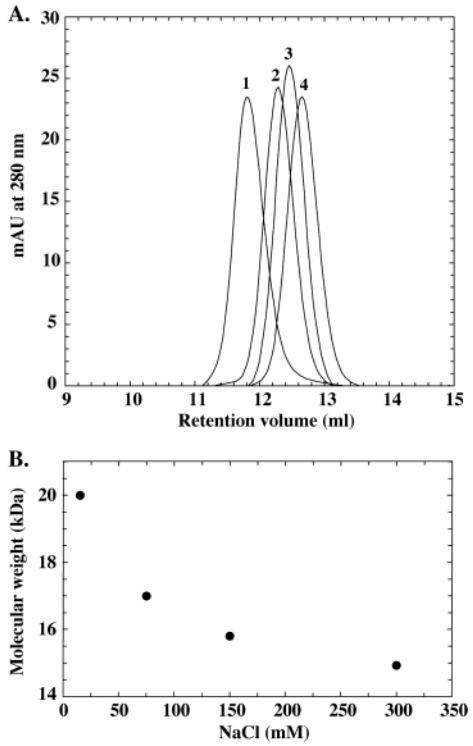

FIGURE 1: Gel filtration chromatography of trHbO. (A) Elution profiles of trHbO-met using a Superdex 75 HR 10/30 column at 23 °C with (1) 15 mM NaCl, (2) 75 mM NaCl, (3) 150 mM NaCl, and (4) 300 mM NaCl. (B) Apparent molecular mass of trHbO as a function of sodium chloride concentration. The apparent molecular mass decreases from 20 kDa at 15 mM NaCl to 14.9 kDa at 300 mM NaCl. The molecular mass of the monomer is 14.9 kDa.

generated by fitting to a single exponential deviated systematically from the observed decay (middle panel of Figure 2A), but the residuals from the two-exponential fitting (bottom panel of Figure 2A) were nearly random, implying that O_2 combination under these conditions is biphasic with a major rate (∼80% of the total) (k_{on} = 0.11 μM^{-1} s^{-1}) and a faster minority rate (k_{on} = 0.85 μM^{-1} s^{-1}) (Table 1). A nearly homogeneous single rate (∼95% of the total) following apparent first-order kinetics was observed in the combination of O_2 with the deoxy form of the B10Tyr → Phe mutant. The second-order rate constant for the major reaction was 0.067 μM^{-1} s^{-1}, which is close to that observed for the major component of the wild-type protein. The minority rate of binding (less than 5%) is faster and independent of O_2 concentration. The time courses for the combination of O_2 with the CD1Tyr → Phe mutant also indicated nearly a homogeneous (95% of the total) rate indicating a single conformation. Remarkably, the association rate constant was much higher (27-fold) than that of the wild-type protein, indicating that CD1Tyr participates in the modulation of O_2 combination to trHbO.

O_2 Dissociation. A biphasic kinetic event was observed for the wild-type protein upon replacement of the heme-bound O_2 with CO in the absence of dithionite, with the major component contributing 78% (Figure 2B). The O_2 dissociation rate constants thus obtained were very low, 0.0014 and 0.0058 s^{-1}, indicating strong stabilization of the heme-bound O_2.

A single apparently homogeneous kinetic event following first-order kinetics to more than 90% completion was

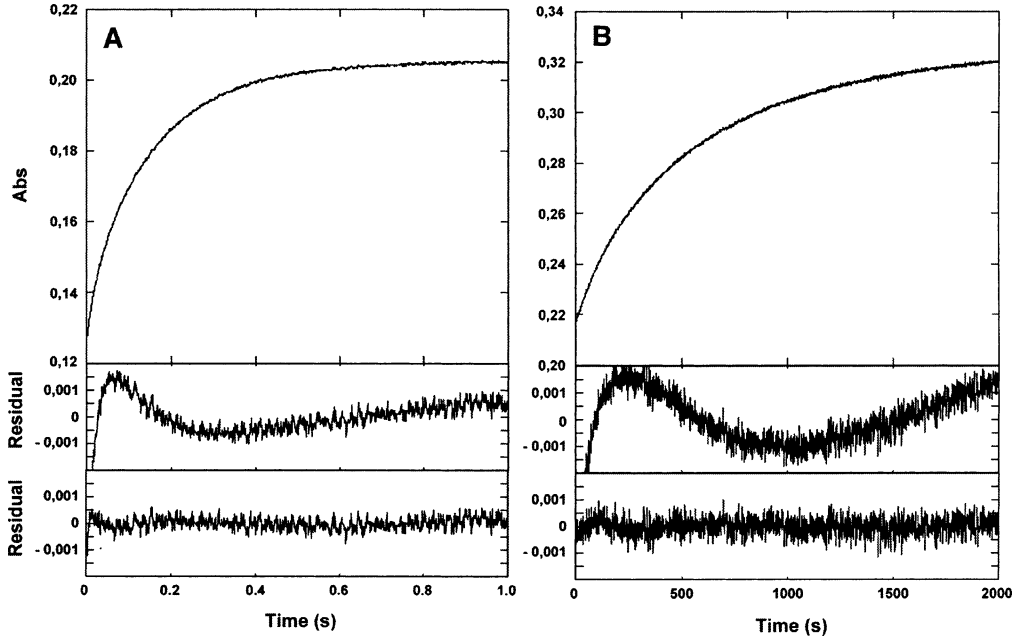

FIGURE 2: O_2 reaction kinetics for wild-type *M. tuberculosis* trHbO. (A) Time course of O_2 combination to wild-type trHbO dissolved in 50 mM phosphate buffer at pH 7.5 and 23 °C. The rate was determined by stopped-flow spectrophotometry (100 μM O_2, before mixing) at 410 nm. (B) O_2 dissociation time courses. The rate was determined by stopped-flow analysis of the time course of replacement of the heme-bound O_2 (10 μM free O_2, before mixing) with 1000 μM CO, before mixing, at 420 nm. Protein samples were 5 μM before mixing. The residuals from the single- and double-exponential fit to the time courses are presented as the bottom traces.

Table 1: Kinetic Constants for the Reactions of Deoxy trHbO with O_2, CO, and NO Compared to Those of Other Proteins[a]

protein (E7/B10/CD1)	$k'_{on}(O_2)$ (μM^{-1} s^{-1})	$k_{off}(O_2)$ (s^{-1})	$l'_{on}(CO)$ (μM^{-1} s^{-1})	$l_{off}(CO)$ (s^{-1})	$k'_{on}(NO)$ (μM^{-1} s^{-1})	ref
trHbO (A/Y/Y)	0.11 (80%)	0.0014 (78%)	0.0137 (79%)	0.0040 (60%)	0.18 (80%)	this work
	0.85 (20%)	0.0058 (22%)	0.180 (21%)	0.0015 (40%)	0.95 (20%)	
trHbO (A/**F**/Y)	0.067 (95%)	0.0026 (50%)	0.013 (95%)	0.023 (56%)		this work
	(5%)[b]	0.0058 (50%)	(5%)[b]	0.0059 (44%)		
trHbO (A/Y/**F**)	2.7 (95%)	0.0093 (75%)	1.06 (95%)	0.0064 (70%)		this work
	11.5 (5%)	0.0052 (25%)	(5%)[b]	0.0015 (30%)		
trHbN (L/Y/F)	25	0.199	6.75	0.005		*6*
trHbN (L/**F**/F)		30				*6*
trGLB3 (A/Y/F)	0.2	0.3	0.014	0.001		*4*
C. eugametos (Q/Y/F)		0.0141[c]		0.0022[c]		*5*
C. eugametos (**G**/Y/F)		0.444[c]				*5*
C. eugametos (Q/**L**/F)		0.948[c]				*5*
Synechocystis (Q/Y/F)	240	0.011	90			*3*, *29*
Synechocystis (Q/**L**/F)		1.25	300			*3*
Paramecium caudatum (Q/Y/F/L)	30.1	25.2	27.7	0.328		*40*
Nostoc commune (Q/H/F//L)	390	79	41	0.01		*7*
Ascaris (Q/Y/F)	1.5	0.004	17	0.018		*30*
myoglobin (H/L/F/L)	14	12	0.51	0.019	20	*33*, *41*
FHb (*E. coli*) (Q/Y/F)	38	0.44	22 (70%)	0.057 (52%)	26 (78%)	*42*
			1.4 (30%)	0.018 (48%)	4 (22%)	
FHb (*E. coli*) (Q/**F**/F)	50	34 (60%)	37 (70%)	0.12 (45%)	33 (70%)	*42*
		3.3 (40%)	1.0 (30%)	0.01 (55%)	2.8 (30%)	

[a] *l* is the rate constant for CO combination. Mutated residues are shown in bold type. [b] Rates are independent of ligand concentration and heterogeneous. [c] Data obtained at pH 9.5.

recorded when dithionite alone (1 mM) was used to trap dissociated O_2. Further analysis revealed that the observed rates were dependent upon dithionite concentration (Figure 3B). No such effect of dithionite concentration was observed for horse heart Mb (Figure 3A). The relation of the observed rate to the dithionite concentration is described by a straight line intercepting the *Y*-axis at a rate value of ~0.004 s^{-1} at 20 °C. This relation may be interpreted as the sum of two rates, one proportional to the dithionite concentration and the other independent of dithionite concentration. The dithionite-dependent rate probably reflects direct reduction of the heme−O_2 complex by dithionite (*27*). The dithionite-independent rate, given by extrapolation to zero dithionite concentration at the *Y*-intercept, may measure the rate of destruction of O_2 molecules by dithionite as they exit the protein matrix.

To confirm the nature of the rapidly accumulated product of the reaction between trHbO−O_2 and dithionite, measurement of the oxygen dissociation rate was repeated in the presence of dithionite and a trapping agent for ferrous deoxy heme proteins, *n*-butylisocyanide (*28*). *n*-Butylisocyanide was used at a concentration of ~20 mM (after mixing), ensuring rapid formation and high occupancy of the formed isocyanide heme complex. The spectrum of the formed product was that

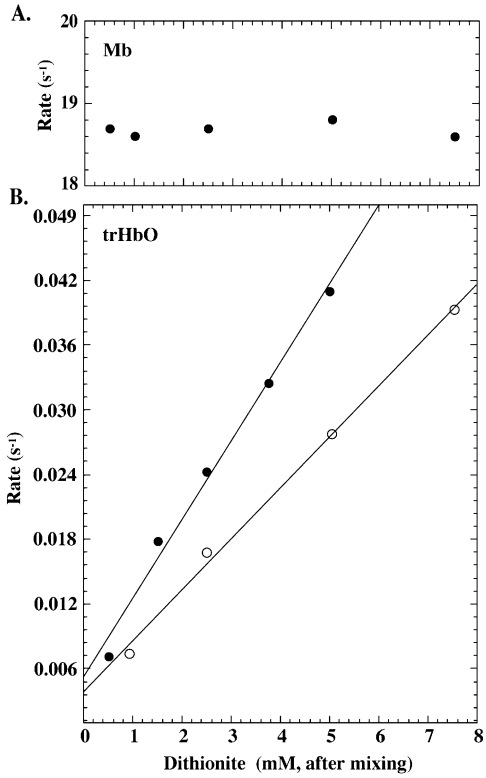

FIGURE 3: Dependence of the dissociation rate of O_2 on the concentration of sodium dithionite. (A) The rate of O_2 dissociation was determined by stopped-flow spectrophotometry, by mixing horse heart Mb−O_2 with solutions containing increasing dithionite concentrations. (B) The rate of O_2 dissociation was determined by stopped-flow methods by mixing trHbO−O_2 with solutions containing increasing dithionite concentrations (○) or with solutions of *n*-butylisocyanide (40 mM, before mixing) containing increasing concentrations of sodium dithionite (●). Those experiments were performed in 50 mM HEPES buffer (pH 7.5).

of authentic ferrous isocyanide trHbO. The ordinate intercept in the plot of dithionite concentration versus reaction rate (Figure 3B) was not changed by the presence of *n*-butylisocyanide. These results indicate that the rapidly accumulated, probably first, product of dithionite reduction is ferrous, deoxy trHbO.

Displacement of O_2 by CO in the B10Tyr → Phe mutant showed two components of almost equal magnitude. The O_2 dissociation rate of the major component (0.0026 s^{-1}) was twice that of the wild type; that of the minor component (0.0058 s^{-1}) was the same as that of the wild type. Displacement of O_2 in the CD1Tyr → Phe mutant was biphasic with the two components contributing in the same proportion as in the wild-type protein. The major O_2 dissociation rate increased 7-fold, suggesting that CD1Tyr participates in the stabilization of the heme-bound O_2. It is noteworthy that changing B10Tyr or CD1Tyr to Phe has only a moderate effect on the dissociation of O_2, the rate of which remains very low. It is also interesting that both mutations have a weak effect on the proportion of the fast and slow reaction rates.

CO Combination. CO binding to wild-type trHbO showed two components exhibiting apparent rate constants, l_{on}, equal to 0.014 (80%) and 0.18 μM^{-1} s^{-1} (20%). As observed for O_2, combination of CO with the deoxy B10Tyr → Phe mutant displayed a nearly homogeneous single component (95% of the total) with a rate constant (l_{on} = 0.013 μM^{-1} s^{-1}) almost identical to that of the major rate of the wild-type protein. CO combination with the CD1Tyr → Phe mutant displayed a single nearly homogeneous major component (95% of total) with a rate constant 78-fold greater than that of the major rate of the wild-type protein.

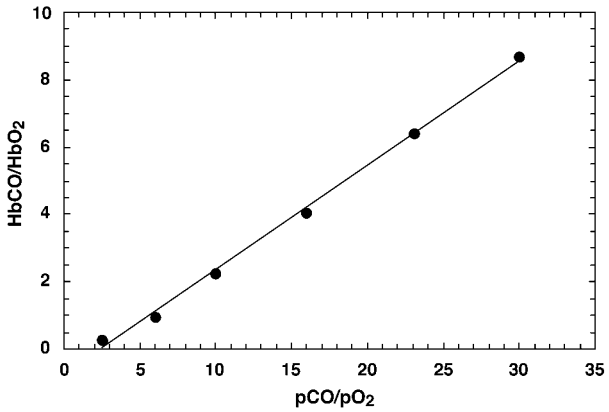

FIGURE 4: Partition of wild-type *M. tuberculosis* trHbO between O_2 and CO. The partition coefficient (M = 0.7) is given by the slope of the line determined by a least-squares fit. This value is expressed in terms of gaseous pressures. A value, M', expressed in molar terms, is related to M by the equation $M' = 1.34M = 0.94$.

CO Dissociation. CO dissociation rate constants were determined by the displacement of CO by O_2. As shown in Table 1, the time course of wild-type trHbO was biphasic with l_{off} values equal to 0.0040 s^{-1} (60% of the reaction) and 0.0015 s^{-1} (40% of the reaction) (Table 1). The time courses of CO displacement for the CD1Tyr → Phe mutant were also biphasic with l_{off} values nearly equal to those measured for the wild-type protein. In contrast, the B10Tyr → Phe mutation resulted in 5.8- and 4.0-fold increases in the CO dissociation rate constants, suggesting that B10Tyr stabilizes the heme-bound CO. As observed for O_2 dissociation, both mutations have very weak effects on the relative proportion of the reactions.

NO Combination. Wild-type deoxy trHbO binds NO in a concentration-dependent manner requiring two exponential terms to fit the pseudo-first-order time courses. The major (80%) and minor (20%) binding reactions give second-order rate constants of 0.18 and 0.95 μM^{-1} s^{-1}, respectively, that are remarkably similar to the values found with O_2.

Partition of Deoxy trHbO between O_2 and CO. The partition coefficient expresses the relative affinity of the protein for CO and O_2. A plot of the [HbCO]/[HbO_2] ratio against the pCO/pO_2 ratio was linear over the range that was examined (Figure 4). The partition coefficient, *M*, expressed in terms of partial pressure, given by the slope of this relation, equals 0.7, which indicates a higher affinity for O_2 than for CO. In contrast, the coefficient partition for trHbN (M = 4.77) indicates a higher affinity for CO than for O_2. Accordingly, cellular roles played by trHbO−O_2 are expected to be less sensitive to CO treatment than those of trHbN.

Time Courses and Rate Constant for the Oxidation of trHbO−O_2 by NO. The low combination rates measured for O_2 and NO suggested that NO-induced oxidation of trHbO−O_2 might be very slow. The reaction of trHbO−O_2 was thus studied by stopped-flow spectrophotometry. Kinetic traces measured at 396 nm resulted in the slow appearance of an aquomet form of trHbO without any evidence of intermediate(s). As shown in Figure 5, trHbO−O_2 exhibited time

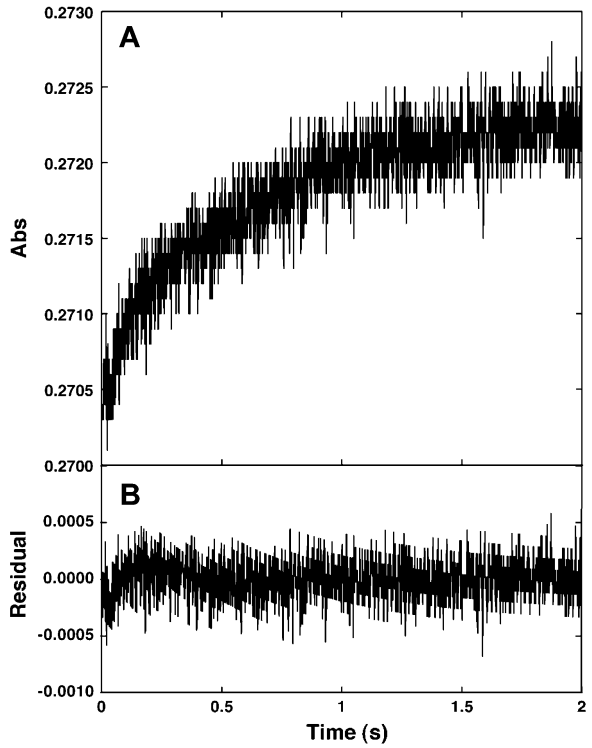

FIGURE 5: Time course for the NO-induced oxidation of trHbO−O_2. (A) Time course (average of six traces) measured at 396 nm for the reaction of 1.0 μM trHbO−O_2 with ~0.1 μM NO at pH 7.5 and 23 °C. (B) The residuals from the single-exponential fit to the time courses are presented.

courses that can be fitted to a single-exponential expression. A plot of the pseudo-first-order rate constants, k_{obs}, versus [trHbO−O_2] was linear with a *y*-intercept of ≈0. The second-order rate constant, obtained from the plots of the pseudo-first-order rate constants, k_{obs}, versus [trHbO−O_2], was 0.6 μM^{-1} s^{-1}. These data show that *in vitro* oxidation of trHbO−O_2 by NO is 1200-fold slower than that of trHbN−O_2.

Photolysis Quantum Yield and Geminate Recombination. Under conditions where samples of Mb−CO are extensively photodissociated using the 8 ns photolysis pulses, we find that at 3.5 °C, comparable (concentration and path length) samples of trHbO−CO cannot be photodissociated. Increasing the temperature results in the progressive appearance of a photoproduct population. The recombination kinetics of a photoproduct population generated at 45 °C are shown in Figure 6. The poor signal-to-noise ratio is a direct result of the low yield of the nanosecond photoproduct even at this elevated temperature. It can be seen that kinetics consist of a fast sub-microsecond recombination and a second much slower recombination extending out into a time regime of hundreds of milliseconds. The fast phase is attributed to geminate recombination. It appears to occur on a time scale that is on the fast end of the distribution of nanosecond to millisecond geminate rates. The slow phase is comparable to the slow CO combination rates reported above. These results suggest that at low temperatures the dissociated CO is highly constrained to remain at the binding site. The high-temperature results show that for those CO molecules that escape from the distal heme pocket, the barrier for recombination is large, consistent with limited access to either the heme or the distal heme pocket.

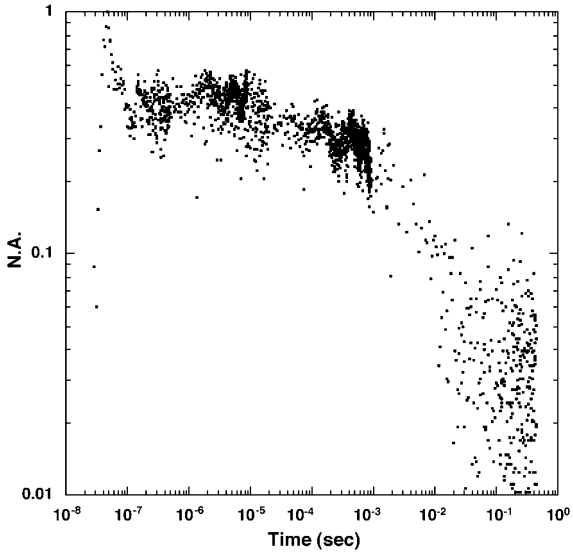

FIGURE 6: Kinetic pattern observed for the recombination of CO with trHbO in a solution at 45 °C. Geminate and solvent phase recombination measurements were carried out using 8 ns pulses as described in Experimental Procedures. The initial QY at the starting temperature of 3.5 °C was close to zero for trHbO.

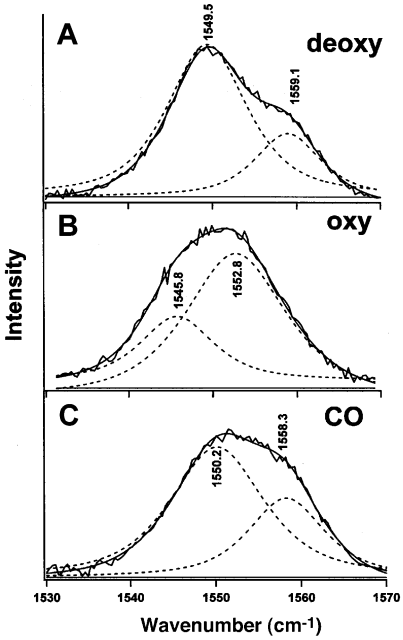

FIGURE 7: UV resonance Raman spectra of deoxy, O_2, and CO derivatives of trHbO. Traces compare the 229 nm-generated W3 band of deoxy (A), O_2 (B), and CO (C) trHbO in solution at ~10 °C. The W3 band of each derivative was deconvoluted into two components using the method described in Experimental Procedures.

UV-Enhanced Resonance Raman Spectroscopy. Figure 7 compares the tryptophan-associated W3 band (generated using 229 nm excitation) for the deoxy, O_2, and CO derivatives of trHbO in solution at ~10 °C. The W3 band is shown deconvoluted into two components. It can be seen that there is a progression in going from deoxy to CO to O_2 in which there is an increase in the ratio of the high-frequency component to the low-frequency component. This ligand- and ligation state-dependent change is much larger than the tryptophan-associated changes reported in the UVRR spectra for either Hbs or Mbs. The results indicate that upon ligand binding the $\chi^{(2,1)}$ dihedral angle for the indole ring increases

from approximately 93° to at least 100°. In addition, the change in the initial (deoxy) population is greater for the O_2 derivative than for the CO derivative. Given the proximity of the G8Trp residue to the binding site and its likely coupling to other ligand binding sensitive distal residues such as B10Tyr and CD1Tyr, we can confidently attribute the changes to G8 and not the other Trp residue that is located between the E and F helices in a domain that helps sequester and water proof the heme within the reduced globin. This result indicates that for trHbO, the heme environment undergoes a conformational change upon ligand binding and that this change is greater for the O_2 ligand than for the CO ligand.

DISCUSSION

Two trHbs, trHbO and trHbN, are expressed in *M. tuberculosis* and *M. bovis*. Here we characterize recombinant trHbO and its complexes with diatomic ligands. Kinetic analysis indicates that binding and dissociation of ligands are achieved quite differently in trHbO and trHbN. In trHbO, ligand binding involves the novel heme distal residues CD1Tyr and G8Trp. trHbO is a noninteracting dimer at low ionic strengths and becomes largely monomeric at higher ionic strengths, where the reported experiments were performed.

O_2 Binding. If only the majority components are considered, the rate of combination of wild-type trHbO with O_2 is ~220-fold lower and the dissociation rate constant is 80-fold lower than that of trHbN. Despite this large difference in the kinetic rate constants, the equilibrium constant K_D for O_2, calculated from the kinetic rate constants, is 12 nM, which is close to that calculated for trHbN (K_D = 8 nM).

Deoxy trHbO. Optical and resonance Raman spectra indicate that ferrous, deoxy *M. tuberculosis* trHbO is pentacoordinate (*10*). Accordingly, the observed slow rate of ligand binding may not be attributed to rate-limiting displacement of a preexisting ligand to the heme iron atom. The outstanding fact is that combination of wild-type trHbO with O_2 and CO is substantially slower than that reported for other trHbs (*5*, *6*, *29*) (Table 1). Two rates, each very slow relative to those of comparable proteins, are seen in O_2, CO, and NO combination: a majority slower rate and a minority rate that is 8-fold (O_2), 15-fold (CO), or 5- fold (NO) faster. The relative proportion of slow and fast components is the same for the three ligands. The rates of both slow and fast components are nearly the same for O_2 and NO, indicating that entry of both ligands is limited by a common steric restraint. Furthermore, the effects of the CD1Tyr → Phe and B10Tyr → Phe mutations on the rates and heterogeneity of CO combination are very similar to those seen for O_2 binding, suggesting that similar mechanisms may govern CO and O_2 combination. Recently, Visca et al. (*2*) reported that CO combination to *M. leprae* trHbO is also heterogeneous with an l_{on} value (0.0073 μM^{-1} s^{-1}) for the majority reaction close to the value we find for *M. tuberculosis* trHbO.

The novel residue CD1Tyr is required to achieve slow ligand combination, since the CD1Tyr → Phe mutation increases the (majority) rates of reaction with O_2 and CO 25- and 77- fold, respectively. The increased rates of combination of the CD1Tyr mutant cannot be attributed to proximal effects, as the Fe−His stretching modes of the ligated and ligand-free forms are the same (*10*).

The novel residue G8Trp is also implicated in the proposed H-bond network that resists ligand binding, because UV resonance Raman spectra, reported here, indicate that the tryptophan indole ring undergoes ligand-specific rotation from its position in deoxy trHbO to new positions in trHbO−O_2 and trHb−CO. Molecular modeling of deoxy trHbO (Figure 8A) indicates that the CD1Tyr residue could be within H-bonding distance of G8Trp and that both this residue and CD1Tyr could be brought close to the heme iron. We suggest that H-bond interactions lock the heme distal residues CD1Tyr and G8Trp into a conformation(s) that limits ligand access to the heme distal pocket.

The effects of the B10Tyr → Phe mutation are less dramatic than those of mutation at position CD1. The majority rates of combination of the B10Tyr mutant with oxygen or CO are unchanged, but the reactions now follow homogeneous courses. The minority, faster components are no longer observed, suggesting that H-bonds involving the B10Tyr stabilize the conformation or structural features that favor faster combination rates. Furthermore, resonance Raman spectroscopic studies (*10*) and protein modeling (Figure 8A) indicate that B10Tyr could be H-bonded to the CD1Tyr. These findings, taken together, suggest that a complex network of H-bonding, involving CD1Tyr, G8Trp, and B10Tyr, controls ligand access to the heme pocket of trHbO.

A group II trHb, named GLB3, from the plant *Arabidopsis* has been characterized recently. GLB3 displays slow, homogeneous combination with O_2, with a rate (k_{on} = 0.2 μM^{-1} s^{-1}) nearly identical to that of trHbO (*4*). Like trHbO, GLB3 has B10Tyr, G8Trp, and E7Ala, but has phenylalanine at position CD1. It is possible that, in trHbO, CD1Tyr takes on the role played by B10Tyr in the *Arabidopsis* protein.

Ligated Forms of trHbO. Dissociation of oxygen from wild-type trHbO is notably slow (Table 1), with rates comparable to those measured for *Ascaris* Hb (k_{off} = 0.0041 s^{-1}), *Chlamydomonas* trHb (k_{off} = 0.014 s^{-1}), and *Synechocystis* trHb (k_{off} = 0.011 s^{-1}) (*5*, *29*−*32*). In these cases, networks of H-bonds involving B10Tyr and E7Gln residues stabilize the heme-bound O_2, resulting in very small O_2 dissociation rates. Each of the single-amino acid substitution mutants, B10Tyr → Phe and CD1Tyr → Phe, increases the rate of the majority, slower component of oxygen dissociation, 2- and 7-fold, respectively, indicating that both residues contribute to stabilization of the heme-bound O_2. However, these effects are small in magnitude relative to the effects of disruption of oxygen-inclusive H-bond networks in other proteins, and small relative to the effects of those same mutations on ligand combination. For instance, mutation of B10Tyr or E7Gln in *Chlamydomonas* trHb increases the dissociation rate 70- and 30-fold, respectively, and mutation of B10Tyr to Phe increases the rate of O_2 dissociation 100-fold in *Ascaris* Hb (*5*, *32*). In trHbN, where O_2 is interacting only with B10Tyr, mutation of B10Tyr to Phe brings a 150-fold increase in the k_{off} rate. The still very low dissociation rates observed in single-residue mutants of trHbO suggest that more than one H-bond must be disrupted to produce a large effect. In this regard, resonance Raman data implicate the CD1 tyrosine in a H-bond network, including the proximal oxygen atom of the ligand (*10*), and the predicted

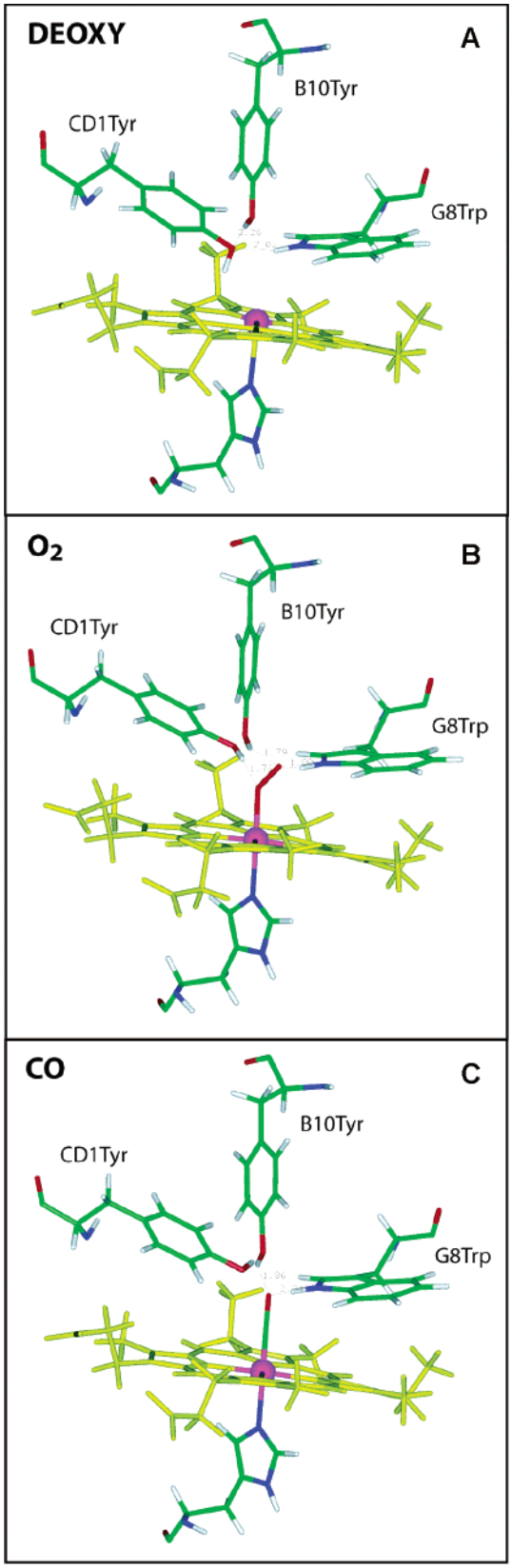

FIGURE 8: Schematic representation of the distal heme pocket of (A) deoxy, (B) O_2, and (C) CO trHbO. The distal heme pocket for deoxy, oxy, and CO trHbO has been produced by substitution of the CD1, E7, and G8 residues on the *M. tuberculosis* trHbN protein scaffold. For additional details, see Experimental Procedures.

structure for trHbO−O_2 shows that residues B10, CD1, and G8 can form H-bonds not only to each other but also to the heme-bound O_2 (Figure 8B). Such an H-bond network, involving three residues and the bound O_2, would greatly minimize the probability that the protein would undergo conformational changes allowing transient disruption of the H-bond network to the heme-bound O_2 , thus permitting O_2 to escape. Breaking more than one H-bond at a time may be necessary to observe a large increase in the O_2 dissociation rate in trHbO.

Reduction of trHbO−O_2 by Dithionite. trHbO−O_2 is reduced by dithionite to ferrous deoxy trHbO without prior dissociation of the oxygenous ligand. This is an unusual reaction for an oxygenated hemoglobin, although dithionite reduction of other ligated hemoglobins is commonly encountered, for instance, in reduction of ferryl myoglobin (aquoferric myoglobin or ferric myoglobin cyanide to ferrous myoglobin or ferrous myoglobin cyanide, respectively). To our knowledge, direct reduction of an oxygenated heme protein by dithionite has been encountered heretofore only in the instance of oxyperoxidase (*27*). Possible sources for this anomalous behavior might include an electronic configuration of the oxygenated heme and its immediate environment that differs from that of most other oxy hemoglobins, or an efficient electron conducting pathway probably related to the high content of aromatic residues in the vicinity of the heme.

CO Is Tightly Constrained in the Heme Distal Pocket. The stopped-flow experiments indicate that trHbO releases heme-bound CO slowly in comparison to Mb and other trHbs (Table 1). In line with these observations, we found that trHbO−CO cannot be photodissociated under conditions where Mb−CO is extensively photodissociated. The geminate recombination process is comparable to that observed for Mb mutants that have distal heme pocket substitutions that greatly limit the diffusion of the dissociated ligand away from the heme (e.g., E11Val → Phe) (*33*). The very low observed nanosecond quantum yield is consistent with a distal heme pocket environment that tightly constrains the dissociated ligand at the iron-binding site, and implies picosecond geminate rebinding for the CO. Geminate rebinding on the picosecond time scale is highly atypical for CO and occurs either when the iron-associated barrier is very low as in Mb−CO at very low pH or when the dissociated ligand cannot diffuse or recoil away from the iron, thereby greatly increasing the probability of accessing the transition state for rebinding (*34*−*36*). The increase in the quantum yield with increasing temperature is likely due to thermally induced weakening of the H-bonding network responsible for maintaining the CO near the heme. The pattern seen at 45 °C can be explained in terms of mixed populations (transient or static) having intact and disrupted H-bonding networks. The population with the intact network is responsible for the low quantum yield. The population with the disrupted network allows for CO diffusion away from the iron and out of the distal heme pocket. The fast nanosecond geminate phase is attributed to CO rebinding from within the distal pocket but from a site removed from the immediate vicinity of the iron. Given the rapidity of the nanosecond geminate rebinding, access by CO from the distal heme pocket to the binding site for this population must not be hindered. The very slow solvent phase rebinding is suggestive of a population with restricted access either to the heme or to the distal heme pocket as is observed for Mb single

mutants having either a Tyr or Trp at the B10 position (*16*, *37*).

The structures of carbon monoxy and oxy trHbO differ in the rotation of G8Trp. The pattern of H-bonding to the two ligands also differs. Changing B10Tyr, but not CD1Tyr, increases the rate of CO dissociation significantly to a value close to that observed for Mb or the other trHbs (Table 1). In accordance, molecular modeling (Figure 8C) shows that in trHbO the oxygen atom of the heme-bound CO could be H-bonded to both B10Tyr and G8Trp but not CD1Tyr. CD1Tyr is H-bonded to G8Trp. Breaking the interaction between B10Tyr and CO may facilitate CO escape by either influencing the inner barrier controlling the formation of the actual ligand−iron bond or allowing more efficient escape from the distal pocket.

Functional Role of trHbO. The distinct features of the heme active site structures of trHbO and trHbN, their different temporal expression patterns, and their ligand binding kinetics suggest that these two trHbs have very different physiological functions. The very high affinity of trHbO for O_2 (nanomolar range) coupled to the very slow release of O_2 makes unlikely that its function is the uptake and delivery of O_2. In addition, the slow oxidation of NO by trHbO−O_2 (0.6 μM^{-1} s^{-1}) in comparison to the oxidation of trHbN (745 μM^{-1} s^{-1}) and that of myoglobin (35−45 μM^{-1} s^{-1}) also makes a NO detoxification role for trHbO unlikely. The low bimolecular rate constant of the reaction of trHbO−O_2 with NO, which is very similar to those measured for NO, CO, and O_2 combination, argues that NO diffusion into the active site is rate-limiting.

The study presented here shows that O_2, NO, and CO all combine with ferrous deoxy trHbO at similar very slow rates. These slow ligand-independent combination rates indicate that the electronic factors that give rise to the large ligand-specific differences in most Mbs and Hbs are not operative. Instead, this result is most consistent with the combination rate being limited by intraprotein diffusion. Similarly, the comparable slow rate for the reaction of NO with heme-bound O_2 of trHbO−O_2 demonstrates that access of small molecules to heme-bound ligands is also limited by the unusually slow intraprotein diffusion.

The off rates for O_2 and CO are found to be comparable for trHbO. This finding is also atypical in that O_2 usually exhibits a much higher off rate than CO. This very low off rate for O_2 is readily ascribed to the presence of multiple hydrogen bonds that both stabilize the bound O_2 directly and minimize hydrogen bond breaking conformational fluctuations. A clear consequence of the very low on and off rates is that oxygen uptake and delivery are not plausible functions for this heme protein. That the binding parameters are essentially ligand-independent indicates that trHbO does not discriminate among ligands. Consequently, in an environment with more than one type of ligand, the population of trHbO-bound ligands will reflect the relative concentrations of the ligands in the solution. This property is compatible with a functional role that reports the relative concentration of ligands such as NO and O_2.

The ability of dithionite to reduce heme-bound O_2 without the prior dissociation of the O_2 and the presence of a high concentration of aromatic residues in the immediate heme vicinity point to the possibility that highly sequestered ligands may be especially prone to redox reactions. Together, these findings suggest a possible redox-mediated signaling that could be responsive to ligand concentrations.

The presence of the electron rich oxidizable residues CD1Tyr and G8Trp close to the heme-bound O_2 is suggestive of redox activity for trHbO. For instance, substitutions of CD1Phe with either Tyr or Trp in Mb have been shown to promote changes in redox properties (*38*, *39*). Furthermore, direct reduction of trHbO−O_2 to deoxy trHbO implies an unusual redox environment for trHbO−O_2. The observation that the hydrogen bonding network and the positioning of the aromatic distal residues are both ligand- and ligation-dependent raises the possibility of a sensor type role in which the redox properties are modulated by ligand-specific ligation at the heme.

ACKNOWLEDGMENT

We thank Dr. Martino Bolognesi for helpful discussions.

REFERENCES

1. Wittenberg, J. B., Bolognesi, M., Wittenberg, B. A., and Guertin, M. (2002) *J. Biol. Chem. 277*, 871−874.
2. Visca, P., Fabozzi, G., Petrucca, A., Ciaccio, C., Coletta, M., De Sanctis, G., Bolognesi, M., Milani, M., and Ascenzi, P. (2002) *Biochem. Biophys. Res. Commun. 294*, 1064−1070.
3. Hvitved, A. N., Trent, J. T., III, Premer, S. A., and Hargrove, M. S. (2001) *J. Biol. Chem. 276*, 34714−34721.
4. Watts, R. A., Hunt, P. W., Hvitved, A. N., Hargrove, M. S., Peacock, W. J., and Dennis, E. S. (2001) *Proc. Natl. Acad. Sci. U.S.A. 98*, 10119−10124.
5. Couture, M., Das, T. K., Lee, H. C., Peisach, J., Rousseau, D. L., Wittenberg, B. A., Wittenberg, J. B., and Guertin, M. (1999) *J. Biol. Chem. 274*, 6898−6910.
6. Couture, M., Yeh, S. R., Wittenberg, B. A., Wittenberg, J. B., Ouellet, Y., Rousseau, D. L., and Guertin, M. (1999) *Proc. Natl. Acad. Sci. U.S.A. 96*, 11223−11228.
7. Thorsteinsson, M. V., Bevan, D. R., Potts, M., Dou, Y., Eich, R. F., Hargrove, M. S., Gibson, Q. H., and Olson, J. S. (1999) *Biochemistry 38*, 2117−2126.
8. Milani, M., Pesce, A., Ouellet, Y., Ascenzi, P., Guertin, M., and Bolognesi, M. (2001) *EMBO J. 20*, 3902−3909.
9. Pesce, A., Couture, M., Dewilde, S., Guertin, M., Yamauchi, K., Ascenzi, P., Moens, L., and Bolognesi, M. (2000) *EMBO J. 19*, 2424−2434.
10. Mukai, M., Savard, P. Y., Ouellet, H., Guertin, M., and Yeh, S. R. (2002) *Biochemistry 41*, 3897−3905.
11. Ouellet, H., Ouellet, Y., Richard, C., Labarre, M., Wittenberg, B., Wittenberg, J., and Guertin, M. (2002) *Proc. Natl. Acad. Sci. U.S.A. 99*, 5902−5907.
12. Pathania, R., Navani, N. K., Gardner, A. M., Gardner, P. R., and Dikshit, K. L. (2002) *Mol. Microbiol. 45*, 1303−1314.
13. Pathania, R., Navani, N. K., Rajamohan, G., and Dikshit, K. L. (2002) *J. Biol. Chem. 277*, 15293−15302.
14. Yeh, S. R., Couture, M., Ouellet, Y., Guertin, M., and Rousseau, D. L. (2000) *J. Biol. Chem. 275*, 1679−1684.
15. Tilton, R. F., Jr., Kuntz, I. D., Jr., and Petsko, G. A. (1984) *Biochemistry 23*, 2849−2857.
16. Draghi, F., Miele, A. E., Travaglini-Allocatelli, C., Vallone, B., Brunori, M., Gibson, Q. H., and Olson, J. S. (2002) *J. Biol. Chem. 277*, 7509−7519.
17. Lamb, D. C., Nienhaus, K., Arcovito, A., Draghi, F., Miele, A. E., Brunori, M., and Nienhaus, G. U. (2002) *J. Biol. Chem. 277*, 11636−11644.
18. Ishikawa, H., Uchida, T., Takahashi, S., Ishimori, K., and Morishima, I. (2001) *Biophys. J. 80*, 1507−1517.
19. Scott, E. E., Gibson, Q. H., and Olson, J. S. (2001) *J. Biol. Chem. 276*, 5177−5188.
20. Srajer, V., Teng, T., Ursby, T., Pradervand, C., Ren, Z., Adachi, S., Schildkamp, W., Bourgeois, D., Wulff, M., and Moffat, K. (1996) *Science 274*, 1726−1729.
21. Thoma, R., Hennig, M., Sterner, R., and Kirschner, K. (2000) *Struct. Folding Des. 8*, 265−276.
22. Trent, J. T., III, Watts, R. A., and Hargrove, M. S. (2001) *J. Biol. Chem. 276*, 30106−30110.

23. Accelrys Inc. (2000) *Insight II*, version 2000.1, San Diego.
24. Arndt, K. M., Muller, K. M., and Pluckthun, A. (1998) *Biochemistry 37*, 12918−12926.
25. Gallagher, C. N., and Huber, R. E. (1997) *Biochemistry 36*, 1281−1286.
26. Zimmerman, J. K., and Ackers, G. K. (1971) *J. Biol. Chem. 246*, 7289−7292.
27. Wittenberg, J. B., Noble, R. W., Wittenberg, B. A., Antonini, E., Brunori, M., and Wyman, J. (1967) *J. Biol. Chem. 242*, 626−634.
28. Gibson, Q. H., Olson, J. S., McKinnie, R. E., and Rohlfs, R. J. (1986) *J. Biol. Chem. 261*, 10228−10239.
29. Couture, M., Das, T. K., Savard, P. Y., Ouellet, Y., Wittenberg, J. B., Wittenberg, B. A., Rousseau, D. L., and Guertin, M. (2000) *Eur. J. Biochem. 267*, 4770−4780.
30. Gibson, Q. H., and Smith, M. H. (1965) *Proc. R. Soc. London, Ser. B 163*, 206−214.
31. Gibson, Q. H., Regan, R., Olson, J. S., Carver, T. E., Dixon, B., Pohajdak, B., Sharma, P. K., and Vinogradov, S. N. (1993) *J. Biol. Chem. 268*, 16993−1698.
32. Kloek, A. P., Yang, J., Mathews, F. S., Frieden, C., and Goldberg, D. E. (1994) *J. Biol. Chem. 269*, 2377−2379.
33. Quillin, M. L., Li, T., Olson, J. S., Phillips, G. N., Jr., Dou, Y., Ikeda-Saito, M., Regan, R., Carlson, M., Gibson, Q. H., Li, H., et al. (1995) *J. Mol. Biol. 245*, 416−436.
34. Iben, I. E., Cowen, B. R., Sanches, R., and Friedman, J. M. (1991) *Biophys. J. 59*, 908−919.
35. Gibson, Q. H., Regan, R., Elber, R., Olson, J. S., and Carver, T. E. (1992) *J. Biol. Chem. 267*, 22022−22034.
36. Anfinrud, P. A., Han, C., and Hochstrasser, R. M. (1989) *Proc. Natl. Acad. Sci. U.S.A. 86*, 8387−8391.
37. Dantsker, D., Samuni, U., Friedman, A. J., Yang, M., Ray, A., and Friedman, J. M. (2002) *J. Mol. Biol. 315*, 239−251.
38. Hara, I., Ueno, T., Ozaki, S., Itoh, S., Lee, K., Ueyama, N., and Watanabe, Y. (2001) *J. Biol. Chem. 276*, 36067−36070.
39. Ozaki, S., Hara, I., Matsui, T., and Watanabe, Y. (2001) *Biochemistry 40*, 1044−1052.
40. Das, T. K., Weber, R. E., Dewilde, S., Wittenberg, J. B., Wittenberg, B. A., Yamauchi, K., Van Hauwaert, M. L., Moens, L., and Rousseau, D. L. (2000) *Biochemistry 39*, 14330−14340.
41. Springer, B. A., Egeberg, K. D., Sligar, S. G., Rohlfs, R. J., Mathews, A. J., and Olson, J. S. (1989) *J. Biol. Chem. 264*, 3057−3060.
42. Gardner, A. M., Martin, L. A., Gardner, P. R., Dou, Y., and Olson, J. S. (2000) *J. Biol. Chem. 275*, 12581−12589.

BI0270337